Metasurface optical solar reflectors using AZO transparent conducting oxides for radiative cooling of spacecraft

Kai Sun,[†,‡] Christoph A. Riedel,[†,‡] Yudong Wang,[†,‡] Alessandro Urbani,[¶] Mirko Simeoni,[¶] Sandro Mengali,[¶] Maksim Zalkovskij,[§] Brian Bilenberg,[§] C. H. de Groot,[†] and Otto L. Muskens[*,‡]

Electronics and Computer Science, Faculty of Physical Sciences and Engineering, University of Southampton, Southampton SO17 1BJ, United Kingdom, Physics and Astronomy, Faculty of Physical Sciences and Engineering, University of Southampton, Southampton SO17 1BJ, United Kingdom, Consorzio CREO, SS.17 Località Boschetto I-67100, L'Aquila, Italy, and NIL Technology, Diplomvej 381, 2800 Kongens Lyngby, Denmark

E-mail: O.Muskens@soton.ac.uk

Abstract

Optical Solar Reflectors are devices that combine high reflection for visible wavelengths with a strong emissivity in the infrared. Compared to the conventional rigid quartz tiles used on spacecraft since the 1960s, thin-film solutions can offer a significant advantage in weight, assembly and launch costs. Here, we present a metasurface based approach using an Al-doped

[*]To whom correspondence should be addressed
[†]Electronics
[‡]Physics
[¶]CREO
[§]NILT

ZnO (AZO) transparent conducting oxide as infrared plasmonic material. The AZO is patterned into a metasurface to achieve broad plasmonic resonances with enhanced absorption of electromagnetic radiation in the thermal infrared. In the visible range, the transparent conducting oxide provides low losses for solar radiation, while intrinsic absorption losses in the ultraviolet range are effectively suppressed using a multilayer reflecting coating. The addition of high-emissivity layers to the stack eventually results in comparable emissivity values to the thin plasmonic device, thus defining a window of opportunity for plasmonic absorption as a design strategy for ultrathin devices. The optimized experimental structure achieves solar absorptance (α) of 0.16 and thermal emissivity (ε) of 0.79. Our first prototype demonstrator paves the way for further improvement and large-area fabrication of metasurface solar reflectors, and ultimately their application in space missions.

Keywords

Meta-surface, TCOs, plasmonics, radiative cooling, metamaterial perfect absorber

Optical Solar Reflectors (OSR) play a crucial role in the thermal control of a spacecraft, since they constitute the physical interface between the thermal management system and the space environment. Glued to the external skin of the radiator panels, OSRs are designed to reflect the solar radiation and radiatively dissipate the heat that is generated on board. Conventional OSRs consist of small quartz tiles, which are metallized on the radiator-facing surface. Optically, an OSR is a spectrally selective filter, that reflects the ultraviolet (UV), visible (VIS) and near infrared (NIR) parts of the optical spectrum which correspond to the radiation spectrum of the sun. At the same time, an OSR emits the thermal infrared spectrum corresponding to that of a black body at 300 K. The performance of an OSR is characterized by the two thermo-optical parameters α (solar absorptance) and ε (infrared emissivity), where α is required to be low and ε to be high. Both α and ε must endure the harsh space environment and remain constant across the life-cycle of the spacecraft (typically 15 years for a telecommunications satellite).

In conventional quartz tile OSRs, the quartz absorbs and emits the thermal infrared spectrum, while the metal backreflector reflects the solar radiation. Quartz tiles have excellent thermo-optical properties, that remain unaltered after long exposure to the space environment. However, quartz tiles are prone to break while handling and cannot be applied to curved or bendable radiator panels. Additionally, quartz tiles add a significant amount of weight to the structure, thereby increasing satellite launch costs. An alternative to quartz tiles are Ag-FEP-foils, where the quartz tile is replaced by a flexible foil of fluoro-ethylene polymer (FEP) as infrared emitter. The foils provide flexibility and can be supplied with integrated adhesives. However, Ag-FEP-foils lack the thermo-optical performance and durability of quartz OSRs. Extended exposure to UV radiation and to reactive species such as atomic oxygen makes the foil become brittle and opaque. In general, the rapid ageing of its thermo-optical, mechanical, and electrical properties makes the Ag-FEP-foil unfit for missions in space lasting more than 3-5 years. The assembly and launch costs of OSRs amount to several tens of thousand US dollars per m^2, therefore there is a considerable opportunity for alternative high-tech solutions.

Here, we present a new metamaterial-based strategy for the optical solar reflector (meta-OSR) used in spacecrafts. Metamaterials represent a class of man-made materials that are designed to achieve properties that cannot be easily obtained using conventional materials. Metamaterials and metasurfaces are finding increasing application in ultrathin flat lenses, polarization control, spatial light modulators, spectral filters, infrared sensing and spectroscopy, and blackbody thermal emitters.[1,2] Metamaterials can be used to design perfect absorbers that have close to unit absorbance in a resonant spectral band.[3] Such metamaterial perfect absorber designs have been used to convert blackbody emission into a narrowband spectral band, of interest e.g. for thermo-photovoltaics.

For the OSR application a different design approach is needed as high emissivity over a large spectral bandwidth is required. Broadband metamaterials have been under consideration for application in solar energy harvesting in the visible range. Solutions have been proposed based on multiple narrowband resonators,[4] trapezoidal structures,[5] tapered plasmonic structures like nano-crescents[6] and transformation-optics designs.[7] In addition, material losses form a powerful tool for

increasing spectral bandwidth without the need for multiple resonator structures. Metamaterials based on lossy metals such as tungsten have been proposed for achieving high solar absorption with low room temperature emissivity for use in solar thermal energy harvesting.[8] Transparent conducting oxides (TCOs) are another class of materials with relatively high losses which can produce broad optical resonances in the thermal infrared.[9] While these losses limit conventional metamaterial applications,[10] they provide opportunities for designing broadband OSRs covering the thermal infrared, as is demonstrated in this work.

Next to designing the infrared response, an equally important challenge is to obtain high reflectivity in the UV-visible range (low α). The combination of a high infrared emissivity with low absorption of the solar spectrum poses strong limitations on the materials and designs that can be used. Most conventional metasurfaces exhibit higher-order resonances and radiation trapping through diffraction and Wood's anomalies of the array,[11,12] that can significantly reduce the solar reflectance. The particular material characteristics of TCOs allow to achieve a metasurface design with low solar absorptance.[13–17] By optimizing the free-carrier density, TCOs are used that exhibit a dielectric response in the visible and metallic response in the infrared spectral range.[18,19] For our device, we use Al-doped ZnO (AZO) which has the advantage of being able to be deposited via atomic layer deposition (ALD), offering highly reproducible material properties and thickness control on the nanometer level.[20–26] We present the design of the meta-OSR and discuss experimental results showing a broadband absorption enhancement in the thermal infrared compared to a planar thin film design. The enhancement at a reduced AZO coverage is explained by plasmonic effects in the array of AZO metasurface elements. The unique combination of infrared plasmonics and high visible transparency of TCOs offer a solution as it allows to achieve an infrared active metasurface with only minor influence on the solar spectrum absorption. Overall, the design with inorganic and robust oxide materials results in an ultra-thin metamaterial technology that combines favourable optical performance with good mechanical and resilient properties for applications in spacecraft.

Meta-OSR design

Due to the mixed electric and magnetic nature of radiation, a single electrical resonator much thinner than the wavelength can only absorb up to 50% of the energy of incident radiation. Initial work in the microwave domain by Smith, Padilla and co-workers showed that 100% absorption could be achieved using a combination of electric and magnetic resonators.[27] However, such a design requires careful balancing of reflection and transmission components and a complete cancellation in the far field to achieve perfect absorption. A significant simplification of the design is achieved by placing the resonator close to a metal plane. In this case, the transmission fields are zero and only reflective components need to be considered. Perfect absorption is obtained in a configuration, known as the Salisbury screen, where the metamaterial is positioned at a quarter wavelength distance from the plane.[3,28] Other conditions of perfect absorption can be found for thin spacers where image currents produce an effective magnetic interaction.[29]

The proposed structure is a traditional Salisbury screen consisting of a stack of three layers: the metal back reflector, the dielectric spacer layer and the TCO metasurface. The schematic of the structure is shown in Figure 1a. A square metasurface geometry was chosen based on previous experience with TCO nanoantennas where interaction strength was found to benefit from a high fill factor.[9,16] The back reflector can be made of Ag or Al, both of which are good reflectors in the visible and infrared spectral range. While Ag has the higher average reflectivity in the visible spectrum, it has a band gap at around 350 nm wavelength, thereby increasing absorption in the ultraviolet. Al on the other hand has a lower average reflectivity and weak bandgap absorption at 800 nm. The use of Ag was discarded in our experimental design for reasons of poor adhesion and its sensitivity to oxidation.

The spacer layer of the structure is designed to create constructive interference of the incoming and the reflected radiation at the position of the AZO metasurface. This works similar to a $\lambda/4$-spacer, however due to the strong dispersion of common dielectrics in the infrared and the coupling of the metasurface to induced image charges, the optimum spacer thickness needs to be optimized for each specific design. The permittivity of the spacer material is another important

parameter as it allows some freedom in the design of this interference condition through dispersion, which however has to be balanced against phonon reflection (reststrahlen) bands lowering ε. Infrared transparent materials like fluorides are of interest for their complete lack of phonon bands in the thermal infrared. However fabrication is substantially more complicated and these materials are generally less robust than oxides. In this project we have chosen SiO_2 for its good material properties and its particular dispersion of the dielectric function around the thermal infrared.

The choice of the plasmonic material for the metasurface is critical for the device performance. We make use of Al-doped ZnO (AZO), which is a transparent conducting oxide whose optical properties can be tuned by the carrier concentration. The optical permittivity can be described using a Drude-Lorentz model.[30,31] The combined effect of dielectric spacer and meta-OSR design results in a broad absorption spectrum which can be further optimized by tuning the parameters of the AZO carrier density, spacer thickness and feature size (see Supporting Information). A good compromise between infrared plasmonic response and transparency in the optical solar spectrum is obtained for a carrier density around $2 \times 10^{20}\,\mathrm{cm}^{-3}$.

To illustrate the principle of the design, we compare in Figure 1b the absorption of the meta-OSR design (red curve) with that of the bare AZO metasurface suspended in air (black curve). For the AZO square metasurface in air, we can clearly identify the resonance shape of an antenna mode with peak absorption of up to 50%. Such resonances were observed in earlier studies on TCO antennas on CaF_2 substrates[9,16] and correspond to a plasmonic nature of the optical response. Clearly, the bare AZO metasurface does not provide a sufficiently strong and broadband absorption for the meta-OSR application. The absorption spectrum of the full meta-OSR design (red curve) shows a much higher absorption over a broader bandwidth. The meta-OSR design benefits from an enhanced absorption through fields reflected by the back-reflector, as well as in increased bandwidth due to effects of optical dispersion provided by the SiO_2[32] (see Supporting Information Section S1 for a more technical discussion about this design). The individual contributions of absorption in the AZO metasurface and the SiO_2 spacer are given by the green and cyan curves. Around the sharp infrared vibrational transitions, the AZO and SiO_2 form a hybrid system and en-

ergy dissipation is distributed between the two parts of the system. Absorption inside the Al back reflector (not shown) contributes to less than 2% in the infrared spectral range. Simulations against angle (see Supporting Information Figure S5) show an increase of the long-wavelength emissivity mainly due to longer path lengths in the spacer, which is of benefit for the total performance of the meta-OSR.

The role of AZO carrier density on the resonance profile and resulting value for emissivity ε is presented in Figure 1c,d. We see that increasing the carrier density from 1×10^{20} cm^{-3} to 4×10^{20} cm^{-3} results in changes in the absorption spectrum. For low carrier density, the absorption does not reach a sufficiently high value. For high carrier density, the resonance of the metasurface shifts toward shorter wavelength. In the plot of emissivity versus carrier density, we see that an optimum is achieved for this geometry for a carrier density around 2×10^{20} cm^{-3}. This optimum is confirmed by more extensive numerical studies presented in the Supporting Information Figure S4.

Results and discussion

Meta-OSR devices were fabricated following the procedure described in the Experimental section. Figure 1e shows a scanning electron microscopy (SEM) cross-section of the thin-film OSR stack, while the top view of the patterned meta-OSR is shown in Figure 1f. The combination of deposition processes, patterning and etching resulted in high quality stacks with good mechanical adhesion of the different materials. The ALD process was tuned to optimize the carrier density of AZO in the metasurface layer. By interleaving Al_2O_3 cycles with several ZnO cycles, referred as a super cycle, the Al content can be tuned and accurately controlled in the deposited film. We investigated the response for AZO with Al cycle ratios in the range of 0-5 %. Reflectivity measurements were taken for the thin-film OSR configuration, as shown in Figure 2a. All spectra show characteristic fringes over the visible and NIR part of the spectrum corresponding to modulated absorption by Fabry-Pérot interference in the device stack. This part of the spectrum is found to be largely independent

of the AZO Al-cycle ratio, as the absorption in this range is caused primarily by losses in the metal back-reflector and not in the AZO, which is transparent in the visible and NIR range. The spectra do show a pronounced absorption effect in the UV range, attributed to absorption of the ZnO, where the absorption in the band edge around 350 nm is strongly reduced with increasing Al-cycle ratio. We attribute this change in absorption to Coulomb screening of excitonic states in ZnO with increasing carrier densities.[33,34] Further toward the infrared in the range 2-15 μm wavelength, a transition to strong absorption is observed which gets larger for increasing Al-cycle ratios. This transition is determined by the metallic absorption of doped AZO and forms a sensitive measure of the carrier density. Between 7-12 μm wavelength, strong dispersion of the SiO_2 dielectric spacer results in distortions of the absorption profile of the thin-film due to the presence of strong vibrational transitions. We calculated α and ε from the measured spectra, resulting in the values plotted in Figure 2b as a function of Al cycle ratio. Values of ϵ range from 0.49 to 0.63 and peak at a 3% Al cycle ratio. Detailed comparison of experimental spectra with numerical calculations using a Drude-Lorentz model, resulted in values of the carrier density as shown in Figure 2c. We find values ranging from 6×10^{19} cm^{-3} to 2×10^{20} cm^{-3}.

For the meta-OSR devices we used the optimized Al-cycle ratio of around 3.5%. Experimental spectra for fabricated meta-OSRs are shown in Figure 3a (solid lines) along with calculations (dashed lines) for a gap of 250 nm. Spectra for a gap of 150 nm are shown in the Supporting Information Figure S15. All spectra show similar features to the planar film devices, with a transition from low absorption and Fabry-Pérot fringes in the visible and near-infrared range, to strong absorption above 5 μm wavelength. In the infrared range, the meta-OSRs show an increased absorption compared the corresponding planar thin-film devices. This is remarkable as the fill factor of AZO for the largest feature sizes is around 70% of that of the continuous film. The corresponding increase in absorption, corrected for reduced AZO fill factor, therefore amounts to around 40%. This effect is attributed to plasmonic enhancement of fields inside the AZO as is discussed further below. UV-visible total reflection measurements for the small-area devices are limited to wavelengths >450 nm. In this range, very good agreement is obtained with the numerical simulations.

Very narrow spikes in the simulations correspond to light trapping by diffraction into the guided modes of the structures. These sharp features are washed out in the measured spectra due to limited spectral resolution. The visible-range absorption in Figure 3 closely follows that for the planar thin-films of Figure 2a, indicating that the meta-OSRs do not act as resonators in the visible range.

Values for ε extracted from the spectra are shown in Figure 3b. Compared to the planar film, all meta-OSR samples show an improvement in ε. While the differences in results between the feature sizes is small for the $d = 150$ nm gap case, the $d = 250$ nm gap shows a significant increase of the performance in ε when increasing the feature size from 0.75 μm to 1.35 μm. In fact, results for the $d = 150$ nm and $d = 250$ nm gap approach each other for the largest feature sizes under study. We find a highest value of $\varepsilon = 0.736$. Figure 3c also shows extrapolated values of α obtained by combining the experimental data with that of the planar thin-film device in the UV range. This approximation is justified by the close correspondence of meta-OSR with both the numerical modelling and thin-film experimental results in the experimentally accessible range. We find values of α around 0.2 for all devices under study. As a figure of merit, the ratio of ε/α is of interest as it characterizes the radiative emission over solar absorption capacity of the device. Resulting values of ε/α for our fabricated structure are shown in Figure 3d, using symbols for the experimental values and dashed lines for the simulations. The horizontal black lines represent the experimental values for the planar structure. The experimental data shows values up to 3.5, beating the planar structure for 150 nm gaps with all pattern sizes and for 250 nm gaps with feature sizes of 1150 nm and 1350 nm.

In order to relate the increase in absorption to plasmonic effects in the AZO-metasurface, we investigate the near-field maps in different parts of the spectrum. Figure 4a shows the experimental infrared spectra for the meta-OSRs with 250 gap (solid lines) and for the planar thin-film device (dashed line). The shaded area represents the increased absorption of the meta-OSR compared to the planar thin-film structure. Figure 4b-e show calculated surfaces maps of the optical near field around the AZO for two selected wavelengths of 8 μm and 16 μm and for feature sizes of 750 nm and 1350 nm, respectively. The optical near field maps show a typical half-wave dipolar antenna

profile which corresponds to the main optical resonant mode of the metasurface elements over the bandwidth, as was discussed in Figure 1b. Different wavelengths result in different local field amplitudes depending on the spectral resonance position for the different sized elements. Next to near-field maps, we calculated the dissipated power density for a normalized incident power of 1 W/m^2, which gives the local absorption coefficient Q_{abs} equal to the reciprocal absorption length. The absorption maps include, next to the particle surface, also the top surface of the SiO_2 substrate. We can clearly identify different amounts of absorption inside the AZO, with a profile related to the internal fields inside the particle. At 16 μm wavelength, we see absorption in the SiO_2 substrate directly around the nanoparticle through a mechanism of surface enhanced infrared absorption (SEIRA).[9] The contribution of SEIRA to the overall absorption is a small effect as the volume of the local hotspots is small compared to the total volume of the OSR.

Reported values of $\varepsilon > 0.7$ and $\alpha < 0.2$ are promising, however further improvement of these parameters is highly desirable to reach a competitive technology able to replace existing planar OSR devices. In particular, further suppression of UV-visible losses requires a design modification in order to address the intrinsic UV absorption of the AZO metasurface. A further improvement of the meta-OSR performance can be achieved through application of a multilayer UV-reflector (UVR) coating of sub-micrometer thickness. The UVR was designed to consist of 17 layers of respectively SiO_2 and Ta_2O_5 with a total thickness of 821 nm. This UVR is sufficiently thin to maintain the essential mechanical characteristics of the ultra-thin meta-OSR design. Figure 5a shows the full spectra for the planar thin-film structure both without (black line) and with (red line) the UVR coating. In agreement with the design, the UVR results in a complete suppression of the AZO losses below 400 nm wavelength. Emissivity was characterized using micro-FTIR for all meta-OSRs under study. Figure 5b,c summarizes the results obtained for thin-films and meta-OSRs without and with a UVR coating. We obtain values for ϵ for the meta-OSRs of up to 0.793. Together with values of α of 0.16, we arrive at a figure-of-merit of ε/α of 4.9, which is a substantial improvement compared to the structures without UVR coating.

The additional increase of the infrared emissivity provided by the UVR coating is a result of

simply adding more materials with a high thermal emittance to the stack. Eventually both plasmonic effects and increasing emitter thickness will approach the limit of maximum emissivity, and the additional benefit of plasmonic enhancement is reduced for very thick layers. Already, the planar thin-film OSR shows an increase of ε of up to 0.75 due to the addition of the high-emissivity UVR coating. Our results thus define a window of opportunity for plasmonic enhancement as a strategy in ultrathin OSRs. Further improvement of ε above 0.8 is increasingly difficult to achieve using our current design, mainly due to the dispersion of the permittivity of the SiO_2 spacer. Current studies are guided by practical considerations related to manufacturability of the devices and have not exhausted all possible designs and materials. Further optimization of designs based on this principle appear possible.

As a next step, scaling up of the concepts to larger areas will be an important milestone toward applications. Scalable and cost-effective fabrication will benefit from techniques such as nanoimprint lithography[35] and, for example, replacement of ALD with sputtering, which is a topic of ongoing study. Critical are the durability of materials and the device integrity over the lifetime of the mission.[36] While the prototype stacks in this study have shown excellent mechanical adhesion, future studies on large area and flexible devices will involve a series of tests and qualification of the devices for space applications including mechanical, thermal, UV and radiation resistance. Atomic oxygen (AO) is one of the predominant species affecting material lifetime in low earth orbit spacecraft.[37] Experimental studies indicate that the penetration of AO into TCOs is several hundred nm,[38] which can be mitigated using a thin cladding or UV reflector top coating. Our design furthermore has a tolerance in carrier density of between $1.5 - 4 \times 10^{20}$ cm^{-3}, therefore design of a slightly higher doping level at the beginning-of-life may allow for a gradual degradation of carrier density over the life-cycle.

Next to applications in space, radiative cooling could have potential for terrestrial applications.[39,40] Current designs have not been optimized to avoid atmospheric absorption lines which is a necessary requirement for decoupling from the atmospheric bath and direct cooling to the outer space background. Terrestrial applications benefit from a reduced UV component in the solar spec-

trum, alleviating the need for UV reflecting coatings. Cost-effectiveness, durability, and scalability of the technology will pose a different set of design criteria for terrestrial applications than for the space environment, which could be explored in future work.

Conclusions

We have demonstrated an optical solar reflector based on a metasurface design that reflects solar irradiation and strongly emits heat at room temperature. The use of a transparent conducting oxide allows us to achieve a plasmonic response in the thermal infrared with good transparency in the visible spectral range. The metasurface concept using metal oxides forms a feasible strategy to improve emissivity of thin-film coatings over a broad bandwidth. We experimentally achieve a 10% broadband increase of radiation efficiency of a metasurface thermal emitter compared to an unstructured AZO film, corresponding to a 40% increase when corrected for the reduced volume fraction of AZO. The broadband enhanced response is a substantial and robust effect which places our metasurface device into a technologically relevant regime. The experimental results show good agreement with numerical FDTD simulations. The metasurface design benefits from half-wavelength plasmonic resonances in increasing the optical absorption while achieving a lower area fraction of metal oxide material than for a planar thin-film design. By combining the meta-OSR with a multi-layer UV-reflecting coating of sub-micrometer thickness, the UV absorption loss caused by the AZO metal oxide is completely suppressed. Our best structures achieve values of infrared emittance ε of 0.793 with solar absorption α of 0.16, resulting in a figure of merit of ε/α of 4.9. Further work is needed to combine the technology with flexible foil substrates and achieve large-area fabrication using e.g. nano-imprint techniques. The meta-OSR concept provides a new ultrathin approach to thermal radiators which could eventually replace conventional technologies such as metalized quartz tiles for use in space.

Experimental Section

Fabrication of meta-OSR. The oxide-insulator-metal stack was fabricated on silicon dioxide (SiO_2) coated silicon substrate. An 80 nm aluminum layer was deposited using sputtering, followed by a 1200 nm thick SiO_2 layer obtained by plasma-enhanced chemical vapour deposition (PECVD) at 350 °C. Subsequently, a 100 nm AZO layer and a 10 nm Al_2O_3 capping were deposited by atomic layer deposition (ALD) using a Savannah ALD system at 175 °C. Figure 1e reveals the polycrystalline structure of the deposited AZO. The Al_2O_3 capping layer was required for adhesion with the e-beam resist ZEP520A. The Al_2O_3/AZO layer was subsequently patterned by e-beam lithography using a JEOL JBX-9300 electron beam system and then an ion beam etch (IBE) process using an OIPT IonFab 300 plus system. The etching conditions were set to argon flows of 5 sccm for beam and 12 sccm for the neutralizer, a beam bias of 500 V, a beam current 300 mA, a beam acceleration voltage of 400 V, a sample tilt angle of 20 ° and a chuck rotation rate of 20 rpm. The etching rates were found to be 3.9 nm/min and 17.9 nm/min for Al_2O_3 and AZO, respectively. At the exposed areas, the Al_2O_3 and AZO layers were accurately removed and the resist ZEP was subsequently stripped by an ultrasonic bath in NMP at 50 °C for about 15 minutes. Figure 1f shows a SEM micrograph of the etched square pattern with 1250 nm gap width.

Optical characterization. To measure the emissivity of the patterned and unpatterned thin film structures, infrared reflectance was measured over the range of 2.5 μm - 25μm using an FTIR microscope with a numerical aperture of 0.2 (Thermo-Nicolet Nexus 670, Continuum microscope). A 80 nm aluminum coated SiO_2/Si substrate was used as reference. Solar absorptance of large-area samples was obtained by measuring the VIS/NIR reflectance using a commercial total reflection spectrophotometer (Bentham PVE300) over a range from 300 nm - 2.5 μm. For the small-area meta-OSR devices we developed a total reflection microscope using a 4-inch integrating sphere (Bentham), a supercontinuum light source and spectroscopic detection spanning a wavelength range of 0.45 μm to 2 μm. For total reflectance measurements, a BaO_2 white reference was used.

Numerical modelling. For numerical simulations of meta-OSRs we used both finite element (COMSOL 5.3) and finite-difference time domain (FDTD, Lumerical) modelling. Lumerical

FDTD was used to simulate the broadband spectra, making use of the benefits of the short pulse to achieve a large spectral bandwidth. To improve spectral resolution, the simulation was divided in up to four different spectral regions from 0.2-2.0 μm, 2-5 μm, 5-15 μm and 15-30 μm. For the detailed near-field maps, we used COMSOL finite element modelling, which was confirmed to give identical results to the FDTD in the infrared spectral range. AZO antennas were modelled as squares with rounded top edges using a radius of curvature of 20 nm.

Acknowledgement

This project was financially supported by the European Union through Horizon-2020 project META-REFLECTOR, ID 687303. OM acknowledges support by the EPSRC through projects EP/J016918/1 and EP/M009122/1. The dataset for this work can be found at 10.5258/SOTON/D0283.

Supporting Information Available

The following files are available free of charge. Simulation results including design optimization and performance under oblique incidence, information on the ALD process, the material properties and the UV absorption of our AZO, spectroscopic characterization of meta-OSRs.

This material is available free of charge via the Internet at `http://pubs.acs.org/`.

References

(1) Zheludev, N. I. Z.; Kivshar, Y. S. From metamaterials to metadevices. *Nat. Mater.* **2012**, *11*, 917–924.

(2) Yu, N.; Capasso, F. Flat optics with designer metasurfaces. *Nat. Mater.* **2014**, *13*, 139–150.

(3) Watts, C. M.; Liu, X.; Padilla, W. J. Metamaterial Electromagnetic Wave Absorbers. *Adv. Mater.* **2012**, *24*, OP98–OP120.

(4) Bossard, J. A.; Lin, L.; Yun, S.; Liu, L.; Werner, D. H.; Mayer, T. S. Near-Ideal Optical Metamaterial Absorbers with Super-Octave Bandwidth. *ACS Nano* **2014**, *8*, 1517–1524.

(5) Aydin, K.; Ferry, V. E.; Briggs, R. M.; Atwater, H. A. Broadband Polarization-independent Resonant Light Absorption using Ultrathin Plasmonic Super Absorbers. *Nat. Comm.* **2011**, *2*.

(6) Cheng, Q.; Cui, T. J.; Jiang, W. X.; Cai, B. G. An Omnidirectional Electromagnetic Absorber Made of Metamaterials. *New J. Phys.* **2010**, *12*, 063006.

(7) Aubry, A.; Lei, D. Y.; Fernández-Domínguez, A. I.; Sonnefraud, Y.; Maier, S. A.; Pendry, J. B. Plasmonic Light-Harvesting Devices over the Whole Visible Spectrum. *Nano Lett.* **2010**, *10*, 2574–2579.

(8) Ginn, J.; Shelton, D.; Krenz, P.; Lail, B.; Boreman, G. Altering Infrared Metamaterial Performance through Metal Resonance Damping. *J. Appl. Phys.* **2009**, *105*, 074304.

(9) Abb, M.; Wang, Y.; Papasimakis, N.; de Groot, C. H.; Muskens, O. L. Surface-Enhanced Infrared Spectroscopy Using Metal Oxide Plasmonic Antenna Arrays. *Nano Letters* **2014**, *14*, 346–352.

(10) Khurgin, J. B. Replacing Noble Metals with Alternative Materials in Plasmonics and Metamaterials: How Good an Idea? *Phil. Trans. R. Soc. A.* **2017**, *375*.

(11) Tikhodeev, S. G.; Yablonskii, A. L.; Muljarov, E. A.; Gippius, N. A.; Ishihara, T. Quasiguided modes and optical properties of photonic crystal slabs. *Phys. Rev. B* **2002**, *66*, 045102.

(12) Murai, S.; Verschuuren, M. A.; Lozano, G.; Pirruccio, G.; Rodriguez, S. R. K.; Rivas, J. G. Hybrid plasmonic-photonic modes in diffractive arrays of nanoparticles coupled to light-emitting optical waveguides. *Opt. Express* **2013**, *21*, 4250–4262.

(13) Li, S. Q.; Guo, P.; Zhang, L.; Zhou, W.; Odom, T. W.; Seideman, T.; Ketterson, J. B.;

Chang, R. P. H. Infrared Plasmonics with Indium-Tin-Oxide Nanorod Arrays. *ACS Nano* **2011**, *5*, 9161–9170.

(14) Naik, G. V.; Liu, J.; Kildishev, A. V.; Shalaev, V. M.; Boltasseva, A. Demonstration of Al: ZnO as a Plasmonic Component for Near-Infrared Metamaterials. *Proc. Nat. Acad. Sci.* **2012**, *109*, 8834–8838.

(15) Naik, G. V.; Shalaev, V. M.; Boltasseva, A. Alternative Plasmonic Materials: Beyond Gold and Silver. *Adv. Mater.* **2013**, *25*, 3264–3294.

(16) Gregory, S. A.; Wang, Y.; de Groot, C.; Muskens, O. L. Extreme Subwavelength Metal Oxide Direct and Complementary Metamaterials. *ACS Photonics* **2015**, *2*, 606–614.

(17) Guo, P.; Schaller, R. D.; Ketterson, J. B.; Chang, R. P. H. Ultrafast Switching of Tunable Infrared Plasmons in Indium Tin Oxide Nanorod Arrays with Large Absolute Amplitude. *Nat. Photonics* **2016**, *10*, 267–273.

(18) Kim, J.; Dutta, A.; Naik, G. V.; Giles, A. J.; Bezares, F. J.; Ellis, C. T.; Tischler, J. G.; Mahmoud, A. M.; Caglayan, H.; Glembocki, O. J.; Kildishev, A. V.; Caldwell, J. D.; Boltasseva, A.; Engheta, N. Role of Epsilon-Near-Zero Substrates in the Optical Response of Plasmonic Antennas. *Optica* **2016**, *3*.

(19) Caspani, L.; Kaipurath, R. P. M.; Clerici, M.; Ferrera, M.; Roger, T.; Kim, J.; Kinsey, N.; Pietrzyk, M.; di Falco, A.; Shalaev, V. M.; Boltasseva, A.; Faccio, D. Enhanced Nonlinear Refractive Index in ϵ-Near-Zero Materials. *Phys. Rev. Lett.* **2016**, *116*, 2339016.

(20) Johnson, R. W.; Hultqvist, A.; Bent, S. F. A Brief Review of Atomic Layer Deposition: from Fundamentals to Applications. *Mater. Today* **2014**, *17*, 236–246.

(21) Illiberi, A.; Scherpenborg, R.; Wu, Y.; Roozeboom, F.; Poodt, P. Spatial Atmospheric Atomic Layer Deposition of $Al_xZn_{1-x}O$. *ACS Appl. Mater. Interfaces* **2013**, *5*, 13124–13128.

(22) Tynell, T.; Karppinen, M. Atomic Layer Deposition of ZnO: a Review. *Semicond. Sci. Technol.* **2014**, *29*.

(23) Frölich, A.; Wegener, M. Spectroscopic Characterization of Highly Doped ZnO Films Grown by Atomic-Layer Deposition for Three-dimensional Infrared Metamaterials. *Opt. Mater. Expr.* **2011**, *1*, 883.

(24) Saarenpää, H.; Niemi, T.; Tukiainen, A.; Lemmetyinen, H.; Tkachenko, N. Aluminum Doped Zinc Oxide Films Grown by Atomic Layer Deposition for Organic Photovoltaic Devices. *Sol. En. Mater. Sol. Cells* **2010**, *94*, 1379–1383.

(25) Elam, J. W.; George, S. M. Growth of Zno/Al_2O_3 alloy films using atomic layer deposition techniques. *Chem. Mater.* **2003**, *15*, 1020–1028.

(26) Pradhan, A. K.; Mundle, R. M.; Santiago, K.; Skuza, J. R.; Xiao, B.; Son, K. D.; Bahoura, M.; Cheaito, R.; Hopkins, P. E. Extreme Tunability in Aluminum Doped Zinc Oxide Plasmonic Materials for Near-infrared Appliations. *Sci. Rep.* **2014**, *4*.

(27) Landy, N. I.; Sajuyigbe, S.; Mock, J. J.; Smith, D. R.; Padilla, W. J. Perfect Metamaterial Absorber. *Phys. Rev. Lett.* **2008**, *100*, 207402.

(28) Engheta, N. Thin Absorbing Screens using Metamaterial Surfaces. *IEEE Ant. Prop. Soc. Int. Symp.* **2002**, *2*, 392–395.

(29) Liu, N.; Mesch, M.; Weiss, T.; Hentschel, M.; Giessen, H. Infrared Perfect Absorber and Its Application As Plasmonic Sensor. *Nano Letters* **2010**, *10*, 2342–2348.

(30) Losego, M. D.; Efremenko, A. Y.; Rhodes, C. L.; Cerruti, M. G.; Franzen, S.; Maria, J.-P. Conductive Oxide Thin Films: Model Systems for Understanding and Controlling Surface Plasmon Resonance. *Journal of Applied Physics* **2009**, *106*.

(31) Liu, X.; Park, J.; Kang, J.-H.; Yuan, H.; Cui, Y.; Hwang, H. Y.; Brongersma, M. L. Quantification and Impact of Nonparabolicity of the Conduction Band of Indium Tin Oxide on its Plasmonic Properties. *Applied Physics Letters* **2014**, *105*.

(32) Kitamura, R.; Pilon, L.; Jonasz, M. Optical Constants of Silica Glass from Extreme Ultraviolet to Far Infrared at Near Room Temperature. *Appl. Opt.* **2007**, *46*, 8118–8133.

(33) Versteegh, M. A. M.; Kuis, T.; Stoof, H. T. C.; Dijkhuis, J. I. Ultrafast Screening and Carrier Dynamics in Zno: Theory and Experiment. *Phys. Rev. B* **2011**, *84*, 035207.

(34) Schleife, A.; Rödl, C.; Fuchs, F.; Hannewald, K.; Bechstedt, F. Optical Absorption in Degenerately Doped Semiconductors: Mott Transition or Mahan Excitons? *Phys. Rev. Lett.* **2011**, *107*, 236405.

(35) Kooy, N.; Mohamed, K.; Pin, L.; Guan, O. A Review of Roll-To-Roll Nanoimprint Lithography. *Nanosc. Res. Lett.* **2014**, *9*, 320.

(36) Dunn, B. *Materials and Processes for Spacecraft and High Reliability Applications*; Springer, Switzerland, 2016.

(37) Reddy, M. R. Effect of low earth orbit atomic oxygen on spacecraft materials. *Journal of Materials Science* **1995**, *30*, 281–307.

(38) Wang, W.; Li, C.; Zhang, J.; Diao, X. Effects of atomic oxygen treatment on structures, morphologies and electrical properties of ZnO:Al films. *Appl. Surf. Sci.* **2010**, *256*, 4527 – 4532.

(39) Raman, A.; Abou Anoma, M.; Zhu, L.; Rephaeli, E.; Fan, S. Passive Radiative Cooling below Ambient Air Temperature under Direct Sunlight. *Nature* **2014**, *515*, 540–544.

(40) Zhai, Y.; Ma, Y.; David, S. N.; Zhao, D.; Lou, R.; Tan, G.; Yang, R.; Yin, X. Scalable-manufactured Randomized Glass-Polymer Hybrid Metamaterial for Daytime Radiative Cooling. *Science* **2017**, *355*, 1062–1066.

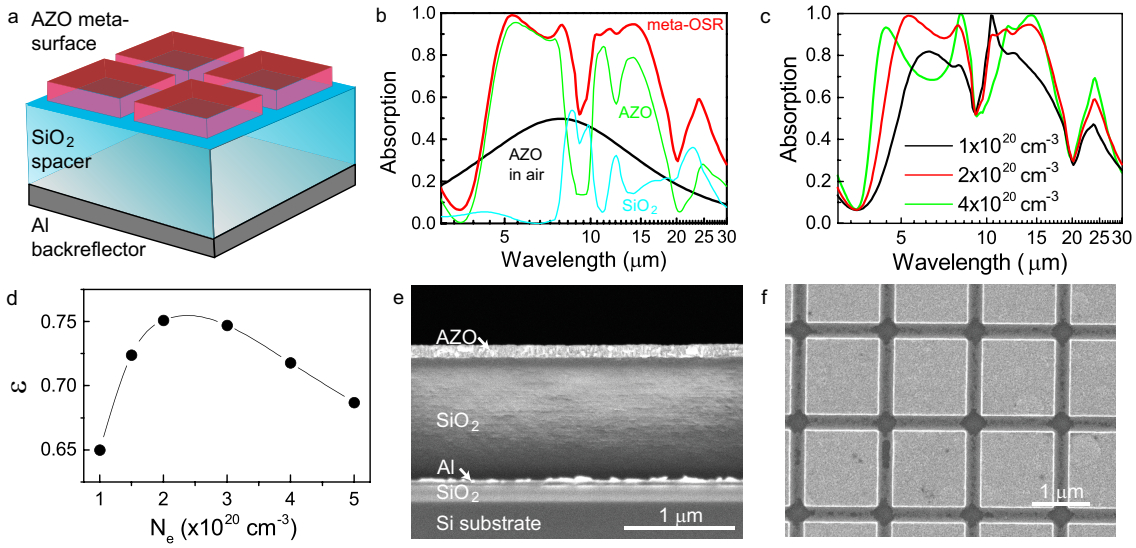

Figure 1: (a) Schematic cross-section of the metareflector design, consisting of Al back-reflector, dielectric (SiO_2) spacer and Al:ZnO (AZO) metasurface. (b) Calculated absorption for AZO meta-surface suspended in air (black) and in meta-OSR (red). Individual contributions of AZO and SiO_2 to the meta-OSR absorption are shown by green and cyan curves, respectively. (c) Absorption spectra of AZO meta-OSR with $L = 1350$ nm, for different carrier densities N_e in the range $1 - 4 \times 10^{20}$ cm^{-3}. (d) Calculated emissivity ε against N_e. (e) SEM cross-section image of a fabricated meta-reflector (planar film region). (f) Planar SEM micrographs of meta-reflectors with feature size of 1350 nm and gap of 250 nm.

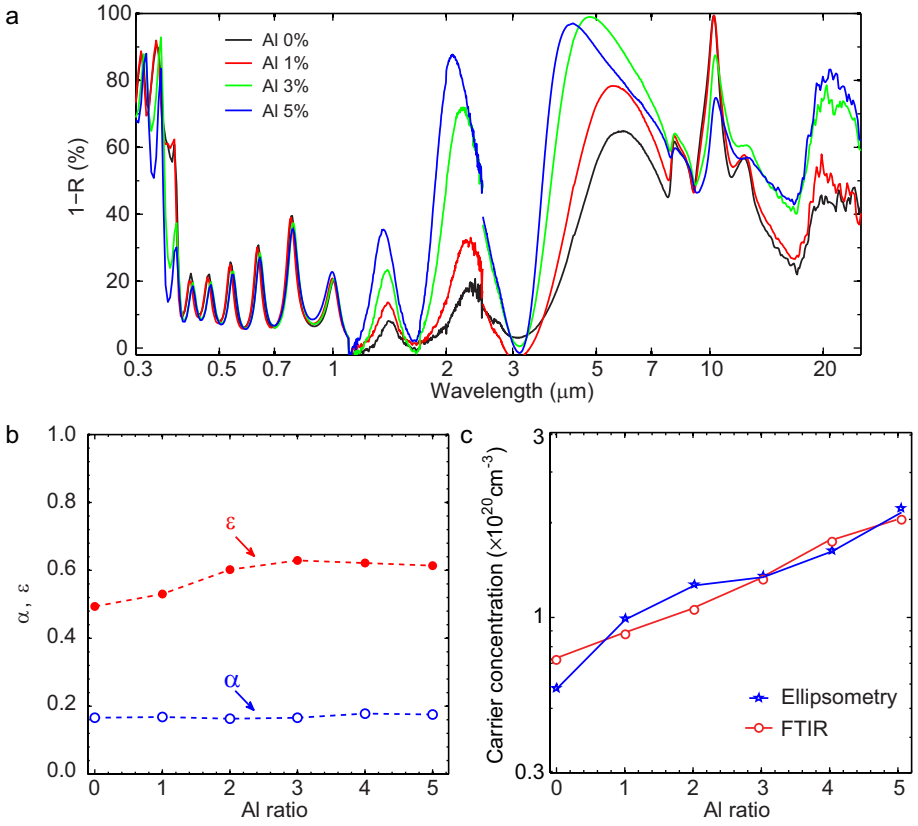

Figure 2: (a) Combined UV-Visible (total reflectance) and infrared (FTIR) spectra of planar AZO film reflectors for different Al ratios from 0% - 5%, showing absorbance $(1 - R)$. (b) Extracted α and ε as a function of Al ratio for the planar film reflectors. (c) Carrier density extracted from ellipsometry (see Supporting Information) and from spectra of (a).

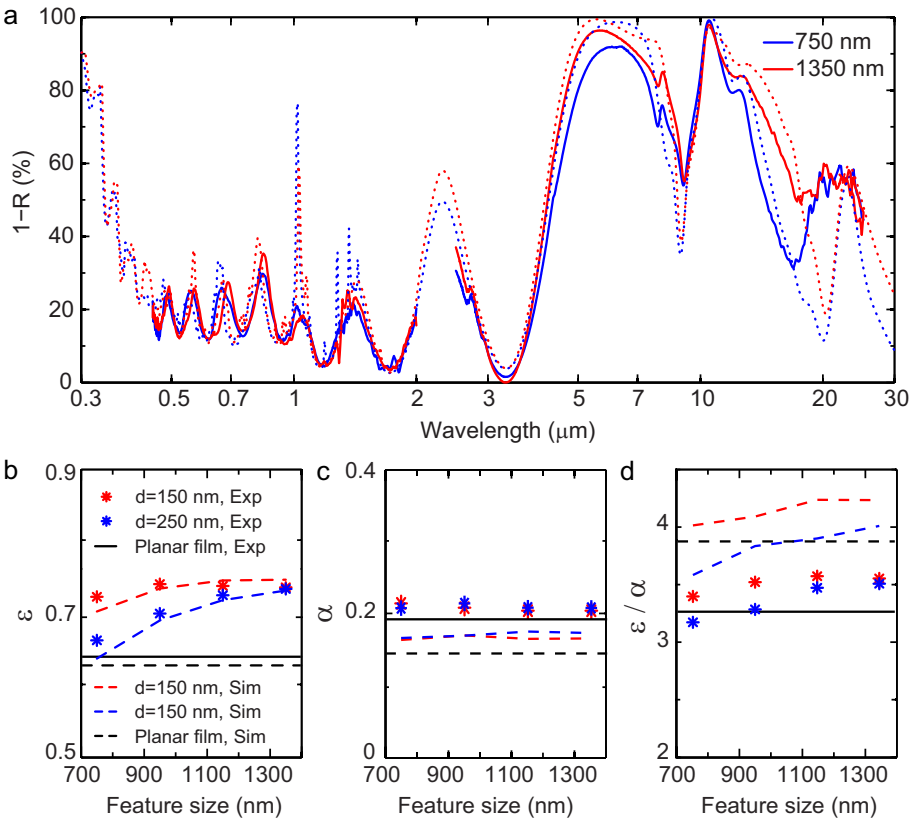

Figure 3: (a,b) Experimental (solid) and simulated (dashed) spectra of AZO meta-reflectors with different feature sizes for 150 nm gap (a) and 250 nm gap (b). The spectra in UV/Vis/NIR and infrared ranges were measured using Quantum emission and FTIR systems, respectively. (c,d) Extracted ε and α (c), and figure-of-merit ε/α (d), as a function of the feature size, for the two gap sizes.

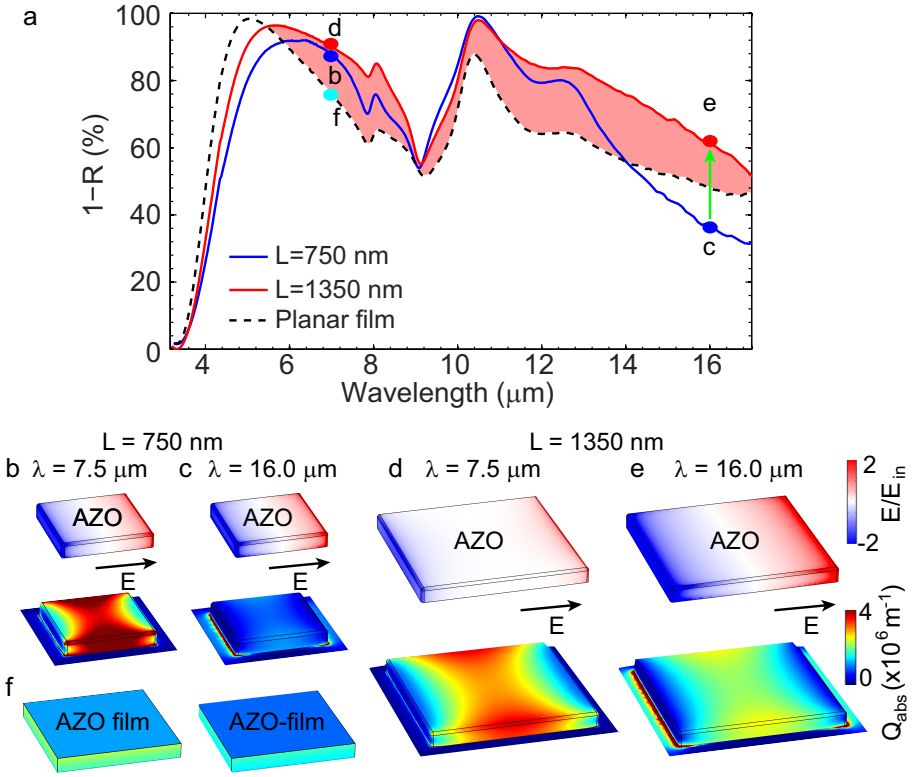

Figure 4: (a) Comparison of experimental infrared spectra of the AZO meta-OSRs with 250 nm gap and the continuous AZO film reflector (dash, black). (b-e) calculated normal near-field ($E/E_{\rm in}$) and absorption coefficient ($Q_{\rm abs}$) at the AZO surface and for wavelengths of 8.0 μm (b,d) and 16.0 μm (c,e) for feature sizes 1350 nm (b,c) and 750 nm (d,e). (f) Absorption coefficient of continuous AZO film.

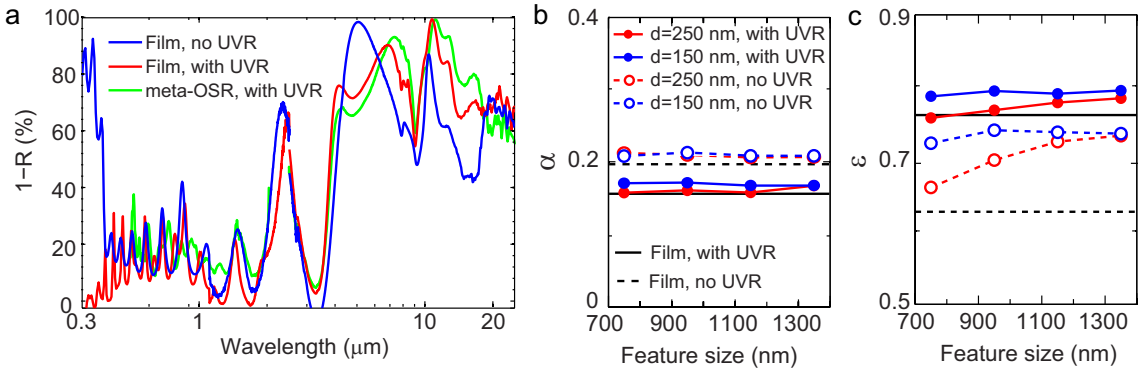

Figure 5: (a) Optical spectra $(1-R)$ for continuous-thin film reflector without (blue) and with (red) UV-reflector (UVR), and for meta-OSR with 1350 nm feature size and 150 nm gap (green). (b) Values of α and ε obtained for thin-film reflector (lines) and for meta-OSRs (symbols, α extrapolated).

Graphical TOC Entry